Optical Anisotropy of a Thermotropic Liquid-Crystalline Polymer in Transient Shear

BENJAMIN S. HSIAO,† RICHARD S. STEIN, KLAUS DEUTSCHER,* and H. HENNING WINTER,* *Polymer Research Institute and *Chemical Engineering Department, University of Massachusetts, Amherst, Massachusetts 01003*

Synopsis

A rheo-optical apparatus, based on a linear shear rheometer, has been constructed to study the deformation of liquid–crystalline polymers. This apparatus uses optical techniques such as flow birefringence, small-angle light scattering, and optical microscopic image analysis. The rheological responses were simultaneously measured under varying temperatures and deformation conditions. The modified Debye-Bueche equation for scattering, in the nonspherically symmetrical form, was adapted to analyze small-angle light-scattering data. The orientation correlation lengths, determined by this method, reveal the deformation mechanism in nematic melts. Flow birefringence results are in agreement with the proposed mechanism.

INTRODUCTION

The rheology of thermotropic liquid-crystalline polymers (LCPs) is of increasing interest in both industrial and academic research. The anisotropic properties of these materials, which are precursors in production of high-modulus and high-strength products (fibers and films), has drawn much attention to them.

The intrinsically ordered structures of the LCP molecules give rise to many unusual rheological phenomena[1-6] such as: a negative first normal stress difference, thermal history effects, shear thinning in the low shear rate region, and so on. These anomalous rheological properties result from the unique morphology of LCPs, which cannot be fully characterized by conventional rheological techniques. It is necessary to utilize rheo-optical methods in monitoring the mesomorphic texture changes during deformation. This rationale has been discussed in detail before.[7]

There are many reports on the rheo-optics of LCPs. Many workers have studied their birefringence[6,8-11] and small-angle light scattering[12,13] during deformation and relaxation. Birefringence measurements alone do not reveal morphological changes. However, they complement polarizing optical microscopy (POM) and small-angle light scattering (SALS), which directly detect morphological changes.

In optical measurements of LCPs, the observed schlieren texture is often interpreted in terms of a disclination network. The concept of a disclination defect, first introduced by Oseen[14] and extended by Frank,[15] is a singularity in a continuous director field based on the continuum theory of curvature elasticity. A nematic state is assumed to consist of a polydomain texture, separated by

---

† Present address: Pioneering Research Laboratory, Fibers Department, Experimental Station, E. I. DuPont Co., Wilmington, DE 19880.

Journal of Polymer Science: Part B: Polymer Physics, Vol. 28, 1571–1588 (1990)
CCC 0887-6266/90/0901571-018$04.00

the spatially distributed disclination lines. These "domains," contain no real physical boundaries, but should be viewed as "effective domains." Within these "domains," the director has an orientational correlation. Average domain size is closely related to the number density and the spatial distribution of the disclinations.

Hashimoto et al.[16,17] and Rojstaczer et al.[18] successfully used polarizing optical microscopy and small-angle light scattering, respectively, to study the kinetics of the coarsening of LCPs schlieren textures. They reported that disclinations were line defects, which contained excess free energy. The disclinations were reduced in number by heat treatment, resulting in the reduction of the average free energy. Free energy reduction was accomplished by increasing the size of the domains. The role of the interaction and spatial distribution of disclinations was discussed in rheological studies of LCPs by Marrucci[19] and Wissbrun.[20] Marrucci assumed a constant number for disclination density during the deformation, whereas Wissbrun implied an increase in disclination density. However, there is little experimental evidence to confirm their arguments.

In this work, we study a thermally stable nematic texture by several optical techniques during linear shear, in order to understand the deformation mechanism of the disclination network. The optical techniques include birefringence, POM, and SALS measurements. SALS is particularly useful in characterizing the orientation correlation lengths within the "effective" domains, which are directly associated with the morphological changes. A medium molecular weight thermotropic LCP system was chosen to avoid possible rheological complexity due to the molecular weight effect. It is believed that high-molecular weight LCPs under high shear rate would exhibit a banded structure during relaxation, whereas lower molecular weight compounds exhibit a much simpler structural change.[21,22] Additionally, a constant shear rate was utilized throughout the various measurements. The specific shear rate was chosen for experimental convenience and to produce rheological behavior characteristic of "region 2."[1,5,23]

EXPERIMENTAL

Material

The thermotropic liquid crystalline polymer is an all-*para*-linked, substituted, wholly aromatic copolyester, which has the chemical structure:

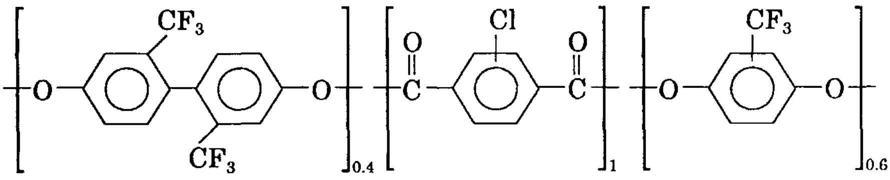

The polymer was synthesized by Polaroid Corp., Cambridge, MA.[24,25] Substituents are placed on the aromatic rings; this forces them into a noncoplanar conformation. Such geometry hinders crystallization, and the material appears completely amorphous. The strong polarizability of the substituents increases the solubility in many solvents.

The glass transition temperature (T_g) of this material is approximately 110°C by differential scanning calorimetry (DSC) at a heating rate of 20 K/min. There is no evidence of a melting transition that can be observed by thermal analysis. The amorphous structure also was confirmed by x-ray results. Above the glass transition temperature, the material exhibited birefringence and remained dimensionally stable. Above 150°C, the material flowed spontaneously yet remained birefringent after cessation of flow. This temperature was chosen as the experimental reference, above which a stable nematic state was obtained. The weight-average molecular weight of this polymer was approximately 24,000, as measured by light scattering from dilute solution.

Sample Preparation

Specimens were prepared with a constant thickness, ranging from 10 to 20 μm, that allows for good optical and rheological responses. The polymer was first ground into a fine powder and vacuum dried at 120°C for 24 h to eliminate moisture. This powder specimen was then pressed between two "Kapton®" films (polyimide from E. I. du Pont) with a 0.002-inch thick brass spacer, under vacuum at 180°C. The recovered film was further compression molded between optical-grade glass surfaces to form a glass-LCP-glass sandwich for the final experiment. The placement of this sandwich is illustrated in Figure 1. A special molder was designed to control the specimen thickness within a 1-μm tolerance. Another type of specimen, such as a glass-LCP-glass-LCP-glass can also be produced by this molder. The latter geometry gives better rheological data.

Instrumentation

A Rheometrics Mechanical Spectrometer (RMS) Model LA (Linear Actuator) rheometer has been modified into a rheo-optical device. This rheometer is capable of measuring a minimum force of 1 g, and operating at shear rates from 10^{-2} to 10^{2} s^{-1}, assuming the sample thickness is 10 μm. A Phase Generator, Model 340, Material Testing Co., was adapted to the RMS for varying rheological measurements. These measurements included constant shear rate, step strain, and dynamic oscillation experiments. A special heating chamber, consisting of a rectangular band heater with windows, was constructed to enclose

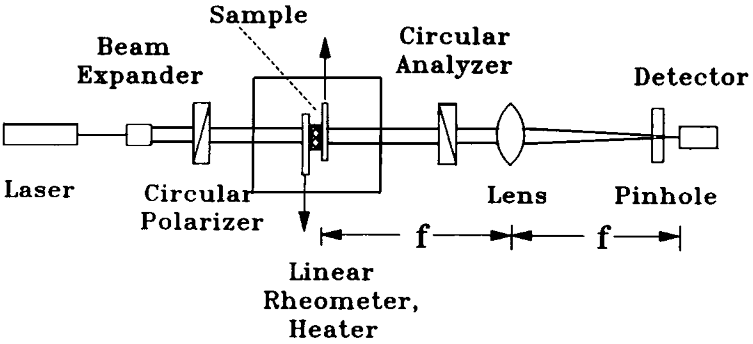

Fig. 1. Rheo-optical setup for measuring birefringence.

the specimen. The heater is able to operate at the maximum temperature of 400°C.

A typical rheo-optical setup for measuring flow birefringence is illustrated in Figure 1. This setup included an 8-mW polarized He-Ne laser, a beam expander, two circular polarizers, a focusing lens, a pinhole, and a laser power detector. The beam expander allowed for measuring a large area of the specimen. The circular polarizer, which consisted of a linear polarizer and a quarter wavelength ($\lambda/4$) plate, were used to eliminate the effect on transmittance of the angular dependence of the specimen optical axis. This system measured the transmittance of the sample during shear. The transmittance is associated with the birefringence, which will be discussed later. A quartz compensator with known birefringence was employed to calibrate this system.

Although a small-angle light-scattering system can be obtained by replacing some of the optical components and the laser power detector with a suitable two-dimensional multichannel detector, no such *in situ* setup was installed for the work reported here. All the specimens were quenched during deformation and investigated by a SALS system that has been described previously.[26] An optical multichannel analyzer (OMA3) (Applied Princeton Research, EG&G, Princeton, NJ), was equipped to study the anisotropic light scattering of the deformed LCPs.

A polarizing optical microscope (POM) equipped with a 35-mm camera, was used to complement the characterization of the quenched specimens. Micrographs were scanned by a Panasonic WV-1850 video camera and the image was sent to a microcomputer equipped with image analysis software for further data processing, such as two-dimensional Fourier transformation (2DFT). The particular software utilized was the SEMPER image processing software (Synoptics, Ltd., Cambridge, England).

OPTICAL TECHNIQUES

Birefringence Measurement

Birefringence was measured by an optical transmission technique.[8-10] For a nonabsorbing, nonscattering, nonreflective, birefringent specimen, the transmittance T_+ for monochromatic light between two crossed circular polarizers is:

$$T_+ = \sin^2(R/2) \qquad (1)$$

where R is the retardation given by

$$R = 2\pi(d/\lambda)\Delta \qquad (2)$$

and d is the sample thickness, λ is the wavelength of the light, and Δ is the birefringence. The application of circular polarizers eliminates the angular dependence of the principal axis to the polarization. The corresponding transmittance $T_{\parallel}$ for monochromatic light between two parallel circular polarizers is

$$T_{\parallel} = 1 - \sin^2(R/2) \tag{3}$$

In the real case, some amount of absorption, reflection, and scattering is always present,[27] and eqs. (1) and (3) should be expressed as:

$$T_+ = F\sin^2(R/2) + T_s \tag{4}$$

$$T_{\parallel} = F(1 - \sin^2(R/2)) + T_s \tag{5}$$

where F is the attenuation of the amplitude due to reflection, absorption, and scattering of the samples. The quantity T_s is the transmission of the sample arising from (a) depolarization of the transmitted beam due to birefringent structures, (b) low-angle scattered light not eliminated from the pinhole, (c) leakage from the polarizers due to incomplete polarization. This quantity can be estimated by measuring the transmittance when the specimen is macroscopically isotropic ($R = 0$), or by measuring the transmittance between crossed linear polarizers at 0° and 90° to the sample optical axis. The quantity F is then calculated by adding eqs. (4) and (5), presuming T_s is known.

Small-Angle Light Scattering

It has been discussed before that when measuring the light scattering from an oriented system, one should use the modified Debye–Bueche equations in the nonspherically symmetrical form.[28] For the cross-polarized condition:

$$I_{Hv}(\mathbf{q}) = KV\langle\eta^2\rangle \int \gamma(\mathbf{r})e^{i(\mathbf{qn})}\, d\mathbf{r} \tag{6}$$

where Hv denotes depolarization (horizontal polarizer, vertical analyzer), K is a constant, V is the scattered volume, $\mathbf{q}$ is the scattering vector whose magnitude is given by $|\mathbf{q}| = (4\pi/\lambda)\sin(\theta/2)$ and $\gamma(\mathbf{r})$ is a correlation function, defined by

$$\gamma(\mathbf{r}) = \langle\eta_i\eta_j\rangle / \langle\eta^2\rangle_{av} \tag{7}$$

In eq. (7), η is the fluctuation in refractive index, $\langle\eta_i\eta_j\rangle_r$ represents the average of $\eta_i\eta_j$ over all pairs of scattering elements i and j separated by a scalar distance r, and $\langle\eta^2\rangle$ represents the mean-square fluctuation in refractive index.

In Cartesian coordinates, the correlation function $\gamma(\mathbf{r})$ depends on the components of $\mathbf{r}$, x, y, and z. Equation (6) can be expressed

$$I_{Hv}(\mathbf{q}) = KV\langle\eta^2\rangle \int \gamma(x, y, z)e^{i(\mathbf{qn})}\, dx\, dy\, dz \tag{8}$$

Considering the case where $\gamma(x, y, z)$ can be factored into independent functions of x, y, and z, one writes

$$\gamma(x, y, z) = \gamma(x)\gamma(y)\gamma(z) \tag{9}$$

This implies that there are no cross correlation terms. Also, the term **qr** can be expressed as

$$\mathbf{qr} = q_x x + q_y y + q_z z \tag{10}$$

where q_x is the x component of $\mathbf{q}$. Equation (8) may be factored into the product of three integrals as

$$I_{Hv}(\mathbf{q}) = KV\langle\eta^2\rangle\tilde{I}(x)\tilde{I}(y)\tilde{I}(z) \tag{11}$$

and

$$\tilde{I}(x) = \int_{-\infty}^{\infty} \gamma(x)e^{i(q_x x)}\, dx \tag{12}$$

$$\tilde{I}(y) = \int_{-\infty}^{\infty} \gamma(y)e^{i(q_y y)}\, dy \tag{13}$$

$$\tilde{I}(z) = \int_{-\infty}^{\infty} \gamma(z)e^{i(q_z z)}\, dz \tag{14}$$

As illustrated in Figure 2, the z direction is that of the incident beam which is normal to the polymer film. The x and y directions are in the film plane, where y direction is the shear direction. Then the scattered intensity $I(\mathbf{q})$ is a function of two angles, θ and μ, defining the orientation of $\mathbf{S}_1$. It is evident from this diagram that

$$\mathbf{q} = (2\pi/\lambda)(\mathbf{S}_1 - \mathbf{S}_0) \tag{15}$$

$$q_x = (2\pi/\lambda)\sin\theta\sin\mu \tag{16}$$

$$q_y = (2\pi/\lambda)\sin\theta\cos\mu \tag{17}$$

$$q_z = (2\pi/\lambda)(\cos\theta - 1) \tag{18}$$

Now, $\cos\theta - 1 = -2\sin^2(\theta/2)$, so at small θ, q_z becomes small compared with q_x and q_y. Hence $e^{i(q_z z)}$ approaches unity more rapidly than do the corresponding

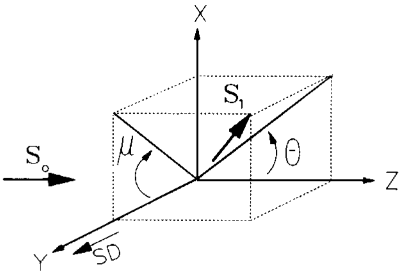

Fig. 2. Small-angle light scattering laboratory coordinate system.

x and y terms. In the case that each individual correlation function can be expressed as a Gaussian

$$\gamma(x) = \exp(-(x/a)^2) \tag{19}$$

$$\gamma(y) = \exp(-(y/b)^2) \tag{20}$$

$$\gamma(z) = \exp(-(z/c)^2) \tag{21}$$

where a, b, and c are characteristic correlation lengths along the x, y, and z directions, respectively. These three correlation lengths characterize the distance over which refractive index fluctuations are correlated in those three directions. At small θ, one can write

$$\tilde{I}(x) = \int_{-\infty}^{\infty} \exp(-(x/a)^2)\exp(i(2\pi/\lambda)x(\sin\theta\sin\mu))\,dx \tag{22}$$

$$\tilde{I}(y) = \int_{-\infty}^{\infty} \exp(-(y/b)^2)\exp(i(2\pi/\lambda)y(\sin\theta\cos\mu))\,dy \tag{23}$$

$$\tilde{I}(z) = \int_{-\infty}^{\infty} \exp(-(z/c)^2)\,dz \tag{24}$$

Thus, at $\mu = 0$ (y direction or shear direction),

$$I_{Hv}(\theta, 0) = KV\langle\eta^2\rangle\pi^{(3/2)}abc(\exp(-(\pi/\lambda)^2b^2\sin^2\theta)) \tag{25}$$

and at $\mu = 90$ (x direction or normal to shear direction),

$$I_{Hv}(\theta, 90) = KV\langle\eta^2\rangle\pi^{(3/2)}abc(\exp(-(\pi/\lambda)^2a^2\sin^2\theta)) \tag{26}$$

It is noted that at small θ, $(\pi/\lambda)^2\sin^2\theta \approx q^2$. Thus, at small angles,

$$I_{Hv}(\theta, 0) = KV\langle\eta^2\rangle\pi^{(3/2)}abc(\exp(-q^2b^2)) \tag{27}$$

$$I_{Hv}(\theta, 90) = KV\langle\eta^2\rangle\pi^{(3/2)}abc(\exp(-q^2a^2)) \tag{28}$$

So a "Guinier" plot of $\ln(I_{Hv}(\theta))$ versus q^2 at $\mu = 0°$ (shear direction) and $\mu = 90°$ (normal to shear direction), respectively, gives the correlation parameters, b and a (the slope represents the square of the correlation distance).

Digital Image Analysis

Optical micrographs of the quenched specimens were digitized by an image analysis computer station. The scanned image was then Fourier transformed in two dimensions (2DFT) and the power spectrum was obtained. In principle, the power spectrum of the POM is different from the small-angle light scattering intensity.[29] This difference is made apparent by the following arguments. The micrograph illustrates the image in real space and the SALS shows the image in $\mathbf{q}$ space, where both images can be expressed by mathematical terms. Under the POM, the image $I_P(\mathbf{r})$ is given by

$$I_P(\mathbf{r}) \cong |\{[\alpha(\mathbf{r})]\mathbf{P}\} \cdot \mathbf{A}|^2 \tag{29}$$

where $\alpha(\mathbf{r})$ is the polarization tensor of the sample, **P** is the unit vector in the direction of the polarizer, and **A** is that in the direction of the analyzer. For SALS, the scattered image $S_P(\mathbf{q})$ is expressed by

$$S_P(\mathbf{q}) = \int_v \langle(\{[\alpha(\mathbf{r})]\mathbf{P}\} \cdot \mathbf{A})(\{[\alpha(\mathbf{O})]\mathbf{P}\} \cdot \mathbf{A})\rangle \exp(-i\mathbf{q}\mathbf{r})\, d\mathbf{r} \tag{30}$$

The power spectrum of any given image in real space can be expressed by

$$P(\mathbf{q}) = \int_v \langle I(\mathbf{r}) I(\mathbf{O})\rangle \exp(-i\mathbf{q}\mathbf{r})\, d\mathbf{r} \tag{31}$$

Therefore, the 2DFT of the optical micrograph is

$$P_P(\mathbf{q}) = \int_v \langle(\{[\alpha(\mathbf{r})]\mathbf{P}\} \cdot \mathbf{A})^2(\{[\alpha(\mathbf{O})]\mathbf{P}\} \cdot \mathbf{A})^2\rangle \exp(-i\mathbf{q}\mathbf{r})\, d\mathbf{r} \tag{32}$$

It is evident that SALS is associated with the second moment of the orientation distribution, whereas the power spectrum of the polarized optical micrograph is associated with the fourth moment.

RESULTS AND DISCUSSION

The rheological characterization of the chosen LCP has been reported elsewhere.[23] It was found that this material had typical "Region 2" shear thinning behavior in the range of shear rates applied (10^{-2} to 10^2 s^{-1}). In this report, only one shear rate (0.25 s^{-1}) is utilized, where good optical and rheological correlations were obtained. The typical rheobirefringent responses of a nematic state at this shear rate are illustrated in Figure 3, in which four different diagrams are presented. Figure 3(a) shows the transient stress response in a start-up flow. It is noted that an overshoot occurs at a strain of less than unity, and a minimum stress is exhibited at a strain of about 40, a value which is dependent on the strain rate. This minimum stress has been observed in many other LCPs,[3,30] and can be associated with the nematic texture deformation. The stress reaches a steady-state value at a strain above 100. Figure 3(b) illustrates the cross-transmitted intensity I_+ and the transmitted intensity amplitude F during the transient state. The intensity F was obtained after the value of T_s was compensated. At the chosen shear rate, T_s varied only slightly with the application of strain and it was determined between crossed linear polarizers at 0° and 90° to the shear direction. When a large shear rate was applied, T_s fluctuated noticeably and had to be calibrated during experiments. It is worthwhile to note that a programmable mechanical (or electronic) stage capable of simultaneously rotating two linear polarizers at various angles with respect to the shear direction and to each other would be ideal for the birefringence measurements, but, was not utilized here. After calibrating for T_s, one can calculate

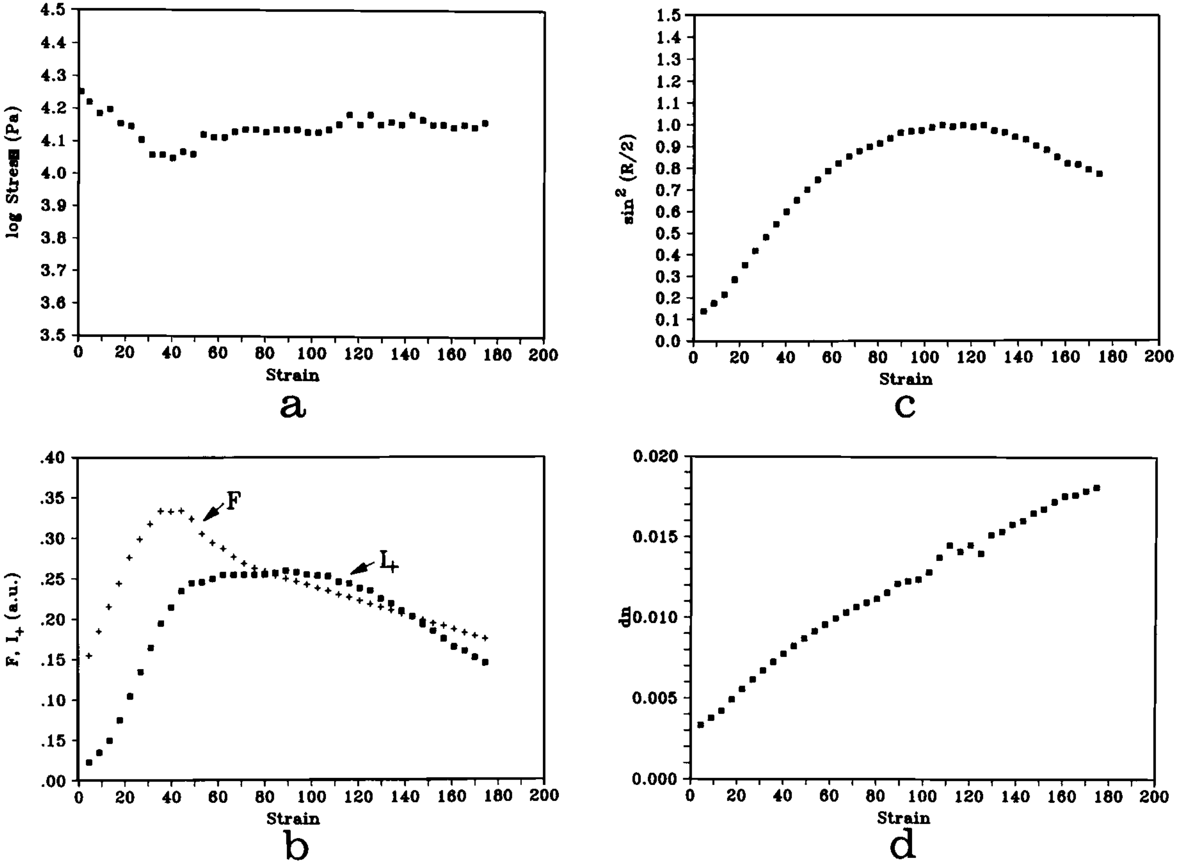

Fig. 3. The rheo-birefringence results of LCP sheared at 0.25 s^{-1} and 160°C; (a) is the stress-strain curve; (b) is the transient transmittance response; (c) is the retardation diagram and (d) is the birefringence.

the retardation value with Eq. (4). This result is shown in Figure 3(c), where $\sin^2(R/2)$ is plotted. It is seen that the retardation undergoes less than one fringe change. By using eq. (2), the flow birefringence has been obtained and is exhibited in Figure 3(d). This birefringence is found to increase continuously with strain, even though the stress has been stabilized. The stress-optical coefficient $(\partial(\Delta n)/\partial\sigma)$ is virtually infinite in this system. Such optical behavior is very different from that of an isotropic fluid, where the stress-optical coefficient usually is constant. Thus, in the nematic state, the strain-optical coefficient $(\partial(\Delta n)/\partial\gamma)$ might be a more useful parameter than the stress-optical coefficient. This behavior is similar to that of crystalline polymers, where the orientation is only increased with strain.[31]

The quenched specimens have been obtained by quickly reducing the temperature below the glass transition temperature. This quenching process was applied with an approximate rate of 40 K/min, at varying strain values. The deformed texture was retained by this quenching process, which was confirmed by deforming the specimen under a polarizing optical microscope. The quenched specimens were then investigated by optical techniques, namely POM and SALS.

Figure 4 shows optical micrographs of the quenched samples deformed at six different strain values. It is clear that the apparent domains are elongated along the shear direction, but remain relatively constant in size in the direction normal to the shear. This schlieren texture can be explained by the spatial arrangement of disclinations. Thus the apparent distance between disclinations is increased in the shear direction, but remains constant in the perpendicular direction, so that disclination density is reduced by shearing. The reduction of the disclination density indicates that the excess free energy is lessened and a more stable state is reached. This observation provides a different perspective than the previous belief that the disclination density either remains constant[19] or is increased[20] during shear.

The same finding has been made by SALS. The results are shown in Figure 5. In this figure, the depolarized (H_v) patterns from the same quenched samples are illustrated. It is noted that the light scattering pattern is elongated along the direction normal to the shear direction and the pattern appears to be ellipsoidal. Since SALS measures the image in $\mathbf{q}$ space, it again suggests that the texture in real space is deformed in the direction of shear.

The polarized scattering pattern (V_v) is the same as the depolarized one (H_v), as can be seen in Figure 6. This indicates that the scattering in this system arises primarily from orientation fluctuations rather than density fluctuations in this system. This conclusion follows because the H_v intensity arises from orientation fluctuations only, whereas V_v arises from a combination of both orientation and density fluctuations.

Figure 7 shows typical plots of scattered intensity versus q (or $|\mathbf{q}|$) for a deformed specimen. The scattered H_v intensity decreases rapidly along the shear direction but decays more gradually perpendicularly to the shear direction. The data are analyzed using a "Guinier" plot, with $\ln I(q)$ plotted against q^2. The slope of the plot is proportional to the square of the orientation correlation distance, b^2 or a^2, in the direction of shear and normal to it, respectively. The resulting plots of orientation distance versus strain at constant shear rate is shown in Figure 8. The upper curve represents the orientation correlation length

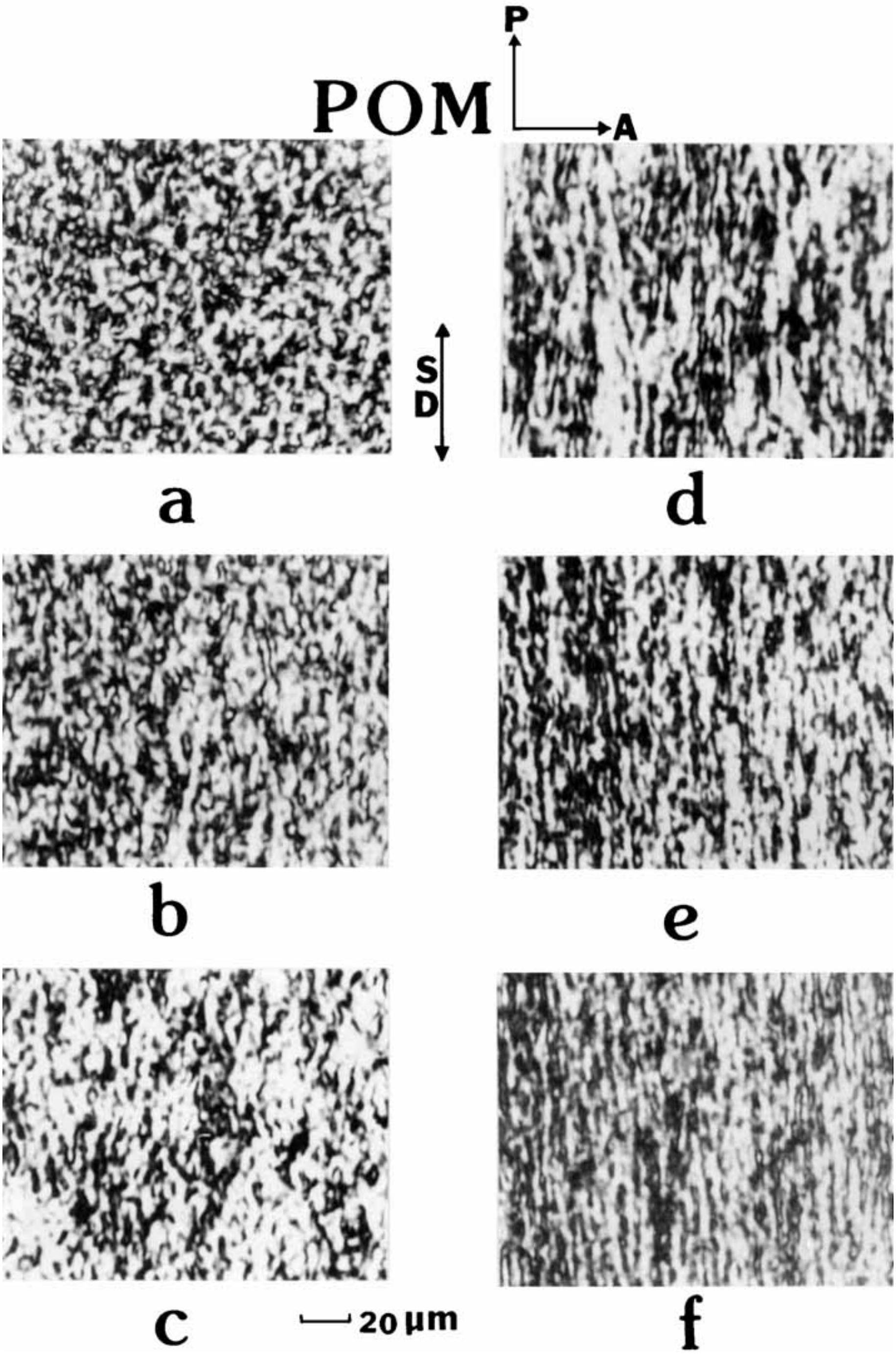

Fig. 4. Polarized optical micrographs (schlieren textures) of deformed specimens quenched at varying strain values. The shear rate is 0.25 s^{-1} and the temperature is 160°C. The strain is (a) 0; (b) 12.5; (c) 35; (d) 50; (e) 102; (f) 193.

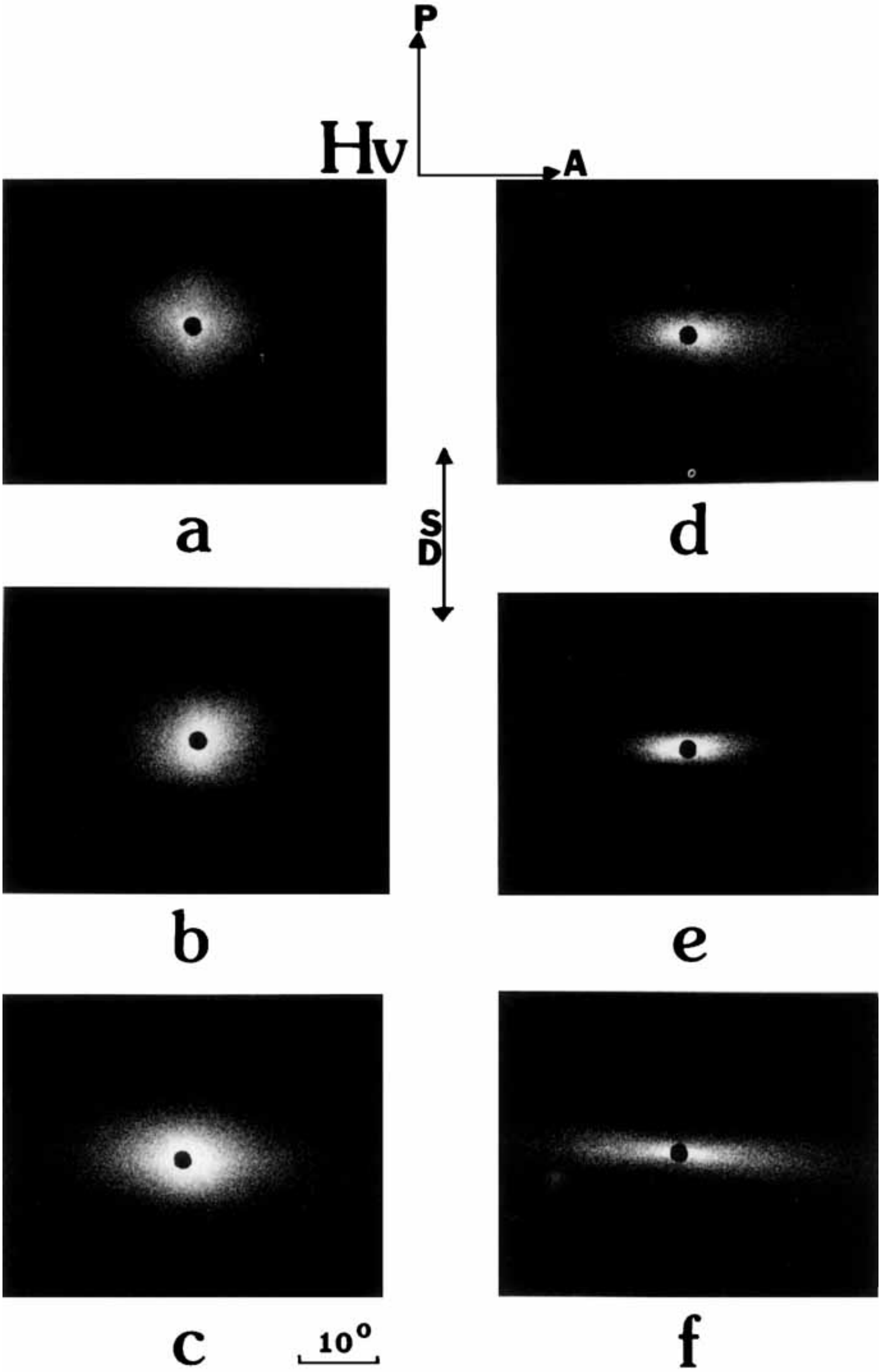

Fig. 5. Depolarized SALS (H_v) patterns of quenched specimens. The condition is the same as Figure 4.

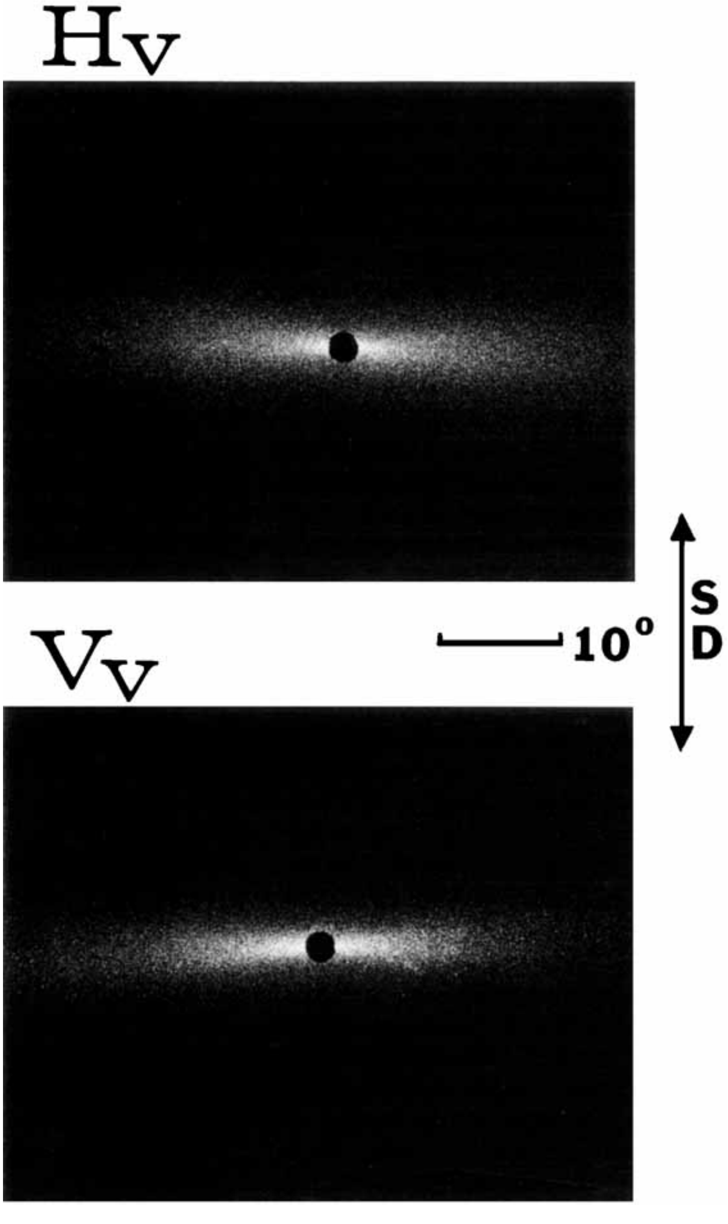

Fig. 6. Polarized (V_v) and depolarized (H_v) SALS pattern of a quenched sample. The temperature is 160°C, shear rate is 0.25 s^{-1} and the strain is about 200.

along the shear direction and the lower curve, that normal to the shear direction. Note, however, that we cannot obtain information about the correlation length in the third direction. It is found that the correlation distance remains constant in the direction normal to the shear. This confirms the previous finding by POM. However, in the shear direction, the orientation correlation length increases with increasing strain and approaches a constant value at strains above

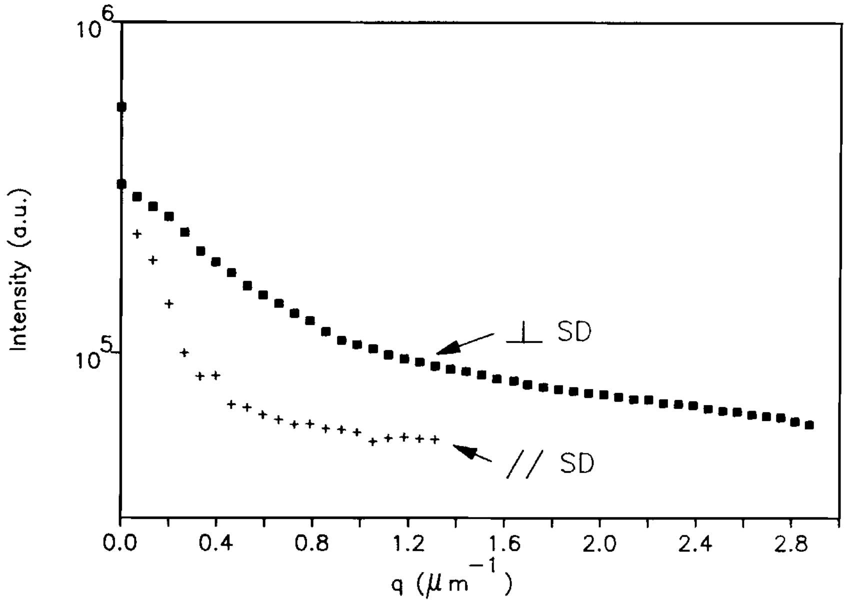

Fig. 7. Scattered H_v intensity vs. q of a typical quenched specimen. The temperature is 160°C, the shear rate is 0.25 s^{-1} and the strain is 50.

100. This compares with the stress–strain measurement, where a steady stress is obtained at the same range of strain.

The calculated value of the correlation length is somewhat different from the value estimated from the optical micrographs. It is apparent that a factor

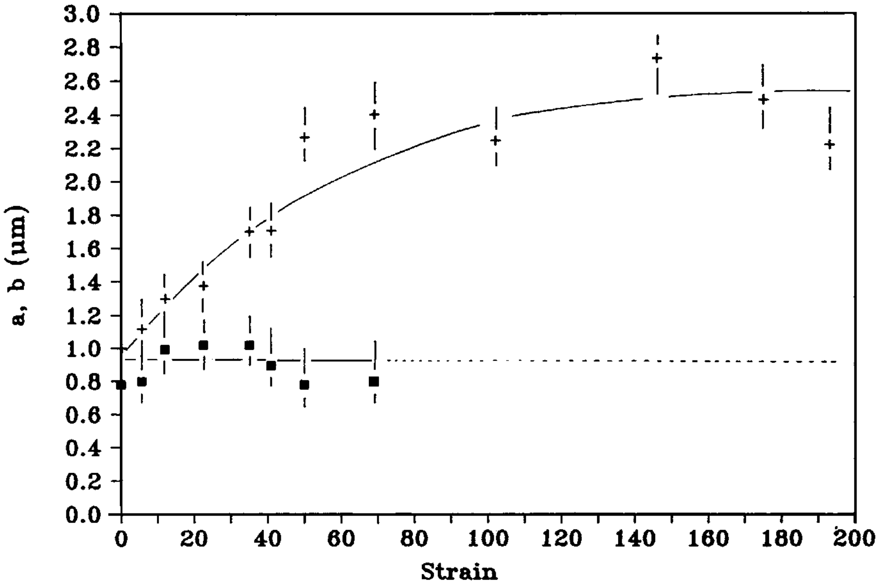

Fig. 8. Orientation correlation lengths, a and b, versus strain. The temperature is 160°C and the shear rate is 0.25 s^{-1}.

should be introduced to correlate the orientation correlation lengths determined by SALS and the texture dimensions from POM.

Figure 9 is a plot of the product of the parallel and perpendicular correlation distances versus strain. This area may be associated with the size of the "effective" domain. An increase of the correlation area indicates an increase of the domain size and a decrease of the disclination density, confirming the observation from optical microscopy. From this figure, it is seen that the domain size approaches a constant value as the strain exceeds 100. Another interesting observation is that the degree of reduction in disclination density is greatest at a strain around 40, where the inflection point is located. At this strain, a minimum stress has been observed before [see Fig. 3(a)], indicating that stress may be directly associated the degree of change in morphological textures.

The optical micrographs of the quenched specimen were converted into a digital image and then transformed into a power spectrum by 2DFT. A typical power spectrum, in the form of an isointensity plot, is shown in Figure 10. In this diagram, the power spectrum image is ellipsoidal. The shape of the power spectrum image is taken to correlate with the texture geometry in real space. This result is shown in Figure 11, where the aspect ratios (*b*/*a*) determined by SALS and the power spectrum, respectively, are plotted against the strain. It is apparent that the aspect ratio of the deformed texture determined by SALS is a stronger function than that measured by the power spectrum. This discrepancy is due to the power dependence of the orientation distribution.

CONCLUSIONS

The deformation of a thermally stable nematic texture was studied with a rheo-optical device. The applied optical techniques included birefringence,

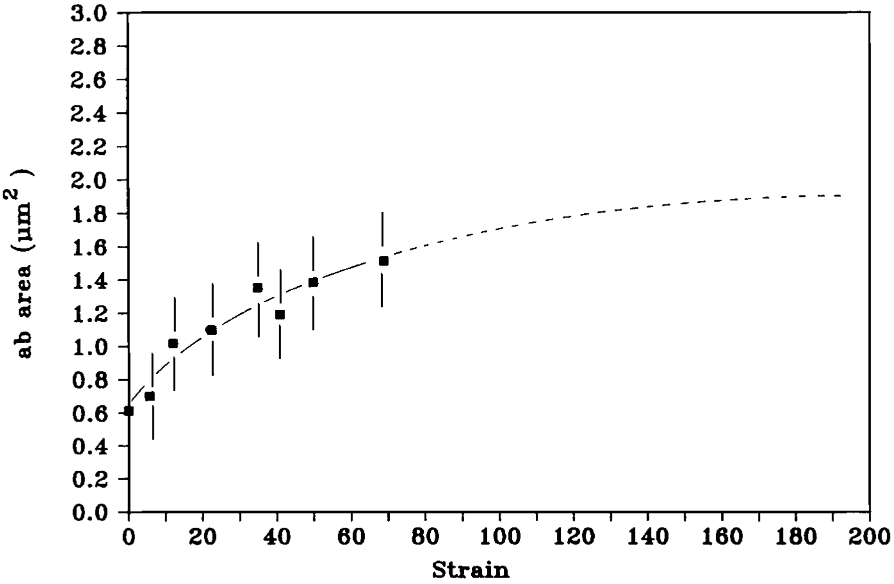

Fig. 9. Product of orientation correlation lengths in Figure 8 versus strain.

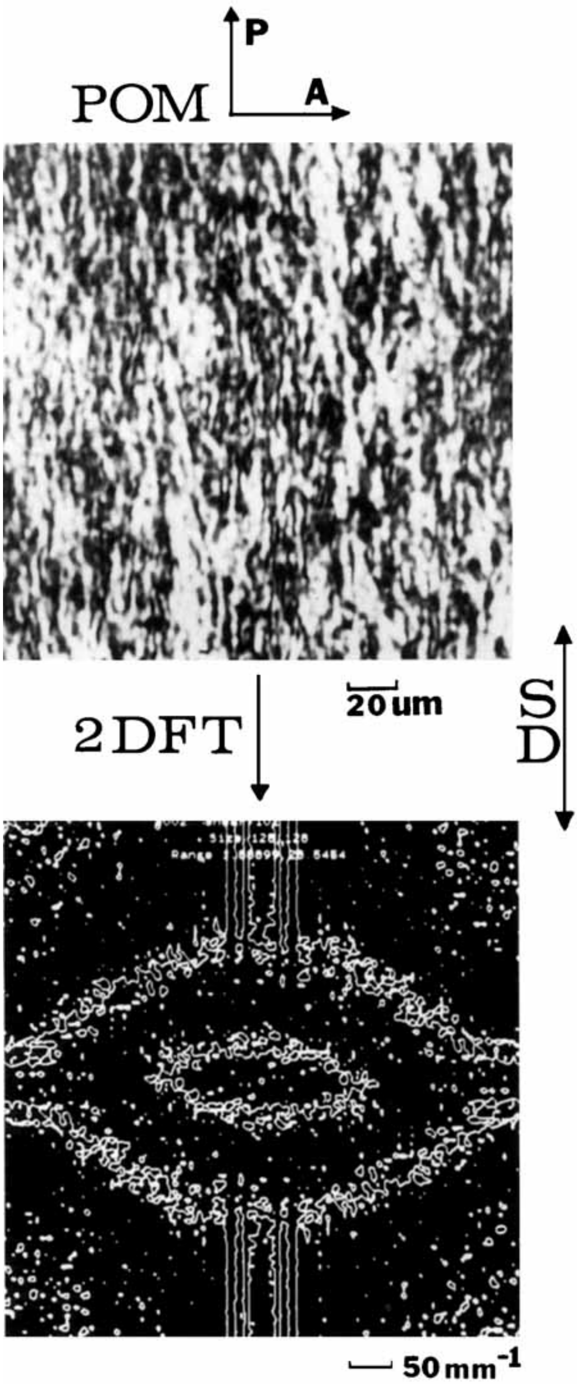

Fig. 10. Typical 2DFT of a POM image and its power spectrum.

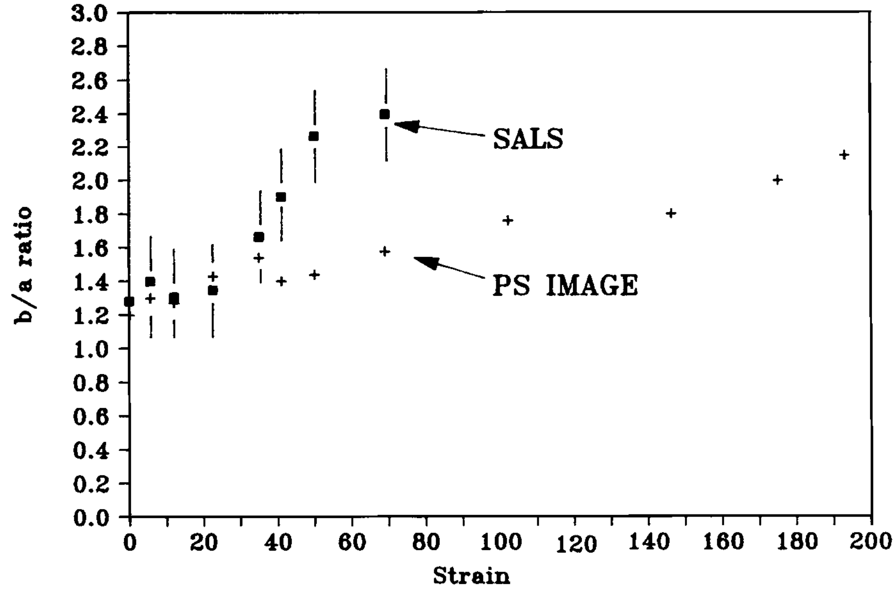

Fig. 11. Comparison of the characteristic aspect ratio of the apparent domain, determined by SALS and the power spectrum, respectively.

small-angle light scattering, and optical image analysis. It was found that birefringence increased as the strain increased, even when the stress remained constant. This indicates the existence of anisotropic structures within the texture, in which the molecular orientation depends not only on the stress, but mainly the strain. This behavior may be contrasted with that of a typical isotropic melt, where the induced orientation is a function of the stress only. In an anisotropic melt, it is preferable to consider the strain-optical coefficient rather than the stress-optical coefficient, as in the case of crystalline systems.

Small-angle light scattering was used to measure the orientation correlation lengths in the shear plane. It was found that the correlation length changed along the shear direction but remained constant normal to the shear. This implies that the texture of the nematic melts was deformed in an anisotropic fashion. It is believed that the orientation correlation length is directly associated with the size of the disclination "domain." One concludes that the number of disclination defects is reduced along the shear direction but remains unchanged in the other directions. The reduction of the disclination density suggests that the excess free energy is lowered, and a more stable state is reached. The optical results from the nematic melts, although they were interpreted by disclination arguments, showed a very similar trend as the crystalline systems.

The characteristic aspect ratio of the deformed "domain" measured by SALS was different from that measured by the optical image analysis technique, because the power spectrum is correlated with the fourth moment of the orientation distribution, while SALS depends on the second moment.

Support for this research from a NSF grant (No. MSM-860-6223) is sincerely appreciated. The authors wish to thank Polaroid Corp., Cambridge, MA., for their gift of material and Dr. S. Rojstaczer, Mr. H. W. Lee, and Mr. K. Schaffer for their technical assistance.

References

1. K. F. Wissbrun, *J. Rheol.,* **25**(6), 619 (1981).

2. G. Kiss and R. S. Porter, *J. Polym. Sci. Polym. Phys. Ed.,* **18,** 361 (1980).

3. G. Viola and D. G. Baird, *J. Rheol.,* **30**(3), 601 (1986).

4. Y. G. Lin and H. Winter, *Macromolecules,* **21,** 2439 (1987).

5. S. Onogi and T. Asada, *Rheology,* Vol I, G. Astarita, G. Marrucci and L. Nicolais (eds.), Plenum Press, New York, 1980, p. 127.

6. Y. Onogi. J. L. White, and J. F. Fellers, *J. Non-Newtonian Fluid Mech.,* **7,** 121 (1980).

7. G. L. Wilkes and R. S. Stein, *J. Polym. Sci. Polym. Symp.,* **60,** 121 (1977).

8. T. Asada, H. Muramatsu, R. Watanabe, and S. Onogi, *Macromolecules,* **13,** 867 (1980).

9. T. Asada, S. Onogi, and H. Yanase, *Polym. Eng. Sci.,* **24**(5), 355 (1984).

10. G. W. Farell and J. F. Fellers, private communications (1988).

11. P. Moldenaers, G. Fuller, and J. Mewis, *Macromolecules,* **22,** 960 (1989).

12. G. C. Berry, *Mol. Cryst. Liq. Cryst.,* **165,** 333 (1988).

13. B. Ernst and P. Navard, *Macromolecules,* **22,** 1419 (1989).

14. C. W. Oseen, *Trans. Faraday Soc.,* **29,** 883 (1933).

15. F. Frank, *Disc. Faraday Soc.,* **25,** 19 (1958).

16. T. Shiwaku, A. Nakai, H. Hasegawa, and T. Hashimoto, *Polym. Commun.,* **28,** 174 (1987).

17. T. Hashimoto, A. Nakai, T. Shiwaku, H. Hasegawa, S. Rojstaczer, and R. S. Stein, *Macromolecules,* **22**(1), 422 (1988).

18. S. Rojstaczer and R. S. Stein, *Mol. Cryst. Liq. Cryst.,* **165** (1988).

19. G. Marrucci, *Proc. IX Congress on Rheol.,* Mexico, 441 (1984).

20. K. Wissbrun, *Faraday Disc. Chem. Soc.,* **79,** 161 (1985).

21. D. J. Graziano and M. R. Mackley, *Mol. Cryst. Liq. Cryst.,* **106,** 73 (1984).

22. N. J. Alderman and M. R. Mackley, *Faraday Disc. Chem. Soc.,* **79,** 149 (1985).

23. S. Bafna, Ph.D. thesis, University of Massachusetts (1989).

24. R. Sinta, R. A. Minns, R. Gaudiana, and H. G. Rogers, *J. Polym. Sci. Part C: Polym. Lett.,* **25,** 11 (1987).

25. R. Sinta, R. A. Minns, R. Gaudiana, and H. G. Rogers, *Macromolecules,* **20,** 2374 (1987).

26. R. J. Tabar, R. S. Stein, and M. B. Long, *J. Polym. Sci. Polym. Phys. Ed.,* **20,** 2041 (1982).

27. S. Kumar and R. S. Stein, *J. Appl. Polym. Sci.,* **34,** 1693 (1987).

28. R. S. Stein and T. Hotta, *J. Appl. Phys.,* **35**(7), 2237 (1964).

29. H. Tanaka, T. Hayashi, and T. Nishi, *J. Appl. Phys.,* **59**(11), 3627 (1986).

30. P. Moldenaers and J. Mewis, *World Congress of Chem. Eng., Polym. Processing,* Tokyo, 546 (1986).

31. R. S. Stein, S. Onogi, K. Sasaguri, and D. A. Keedy, *J. Appl. Phys.,* **34**(1), 80 (1963).

Received May 24, 1989
Accepted December 1, 1989